



Enhanced nitrate removal and fouling behavior in a denitrifying membrane bioreactor: impacts of carbon source and C/N ratio

Zhaozhao Wang^{a,b}, Peng Gao^{a,b}, Lina Yan^c, Chunyu Yin^{a,b}, Simin Li^{a,b,*}

^aCollege of Energy and Environmental Engineering, Hebei University of Engineering, Handan 056038, China, Tel. +8617831917609; emails: 18303233729@163.com (S. Li), W-Z-Z@163.com (Z. Wang), 13082137058@163.com (P. Gao), 13730039533@163.com (C. Yin)

^bCenter for Water Pollution Control and Water Ecological Remediation, Hebei University of Engineering, Handan 056038, China

^cCollege of Environmental and Energy Engineering, Beijing University of Technology, Beijing 100124, China, email: yanlina01@126.com (L. Yan)

Received 30 March 2020; Accepted 29 July 2020

ABSTRACT

The impacts of the carbon source (sodium acetate, ethanol) and C/N ratio (1.0, 3.0, and 5.0) on nitrogen removal and membrane fouling behavior were investigated using a denitrifying membrane bioreactor (DNMBR) treating nitrate-rich wastewater. The results showed that the C/N ratio showed a more significant impact on the process performance than the carbon source. The nitrogen removal efficiency (NRE) was slightly higher when employing sodium acetate as the electron donor at different C/N ratios. The nitrogen removal improved with an increase in the C/N ratio due to the increased specific degradation rate of NO_3^- -N ($\text{SDR}_{\text{NO}_3^-}$); the NRE increased from 24.43% and 13.23% at a C/N ratio of 1.0% to 97.79% and 96.46% at a C/N ratio of 5.0 for the sodium acetate and ethanol systems, respectively. The fouling rate accelerated due to decreased particle size and increased metabolic production, which resulted in the deterioration of sludge rheological properties and dewaterability with an increase in the C/N ratio. The membrane fouling rate with sodium acetate supporting the DNMBR was lower than that of the ethanol system at different C/N ratios, which was attributed to different fouling mechanisms. The high (>100 kDa) carbohydrate molecular weight fraction of soluble microbial production played an important role in membrane pore-blocking in the sodium acetate system. For the ethanol system, the high (>100 kDa) molecular weight protein fraction of extracellular polymeric substances and smaller-sized particles formed a denser cake layer. Fourier transform infrared analysis showed the carbohydrate-like and protein-like substances were the main membrane foulants throughout the entire operation.

Keywords: Denitrification; C/N ratio; Carbon source, Membrane fouling, Sludge characteristics

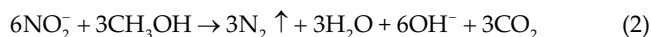
1. Introduction

Nitrate pollution in water bodies is a global concern. Excessive nitrate discharge can stimulate eutrophication in a slow-flow water body, which can lead to the deterioration of water quality and pose a potential threat to human health [1,2]. To enhance nitrate removal, different processes have been developed, such as electrochemical [3], chemical

catalytic [4], and biological denitrification [5]. Among them, biological denitrification is a relatively economical, highly efficient, and stable technology for sewage treatment. Biological denitrification technology refers to the process that converts nitrate or nitrite into dinitrogen by a class of functional bacteria employing a carbon source as an electron donor under anoxic conditions. The specific bioreactions

* Corresponding author.

(here using methanol as the carbon source) are shown in Eqs. (1) and (2):



It can be inferred that the external carbon source is an important factor affecting denitrification efficacy. A few studies have shown that the types of carbon source and C/N ratios significantly affect biological denitrification [6]. Low molecular weight organic matter (e.g., short-chain acids, alcohols, glucose, and digestion supernatant from the primary sedimentation sludge or wasted sludge) have been utilized as carbon sources for biological denitrification [7,8]. Biodegradable polymers and solid organic carbon sources have been attempted as electron donors for denitrification [9,10]. Sodium acetate and ethanol are two typical carbon sources, which are usually employed as the electron donors for the denitrification process in the practical wastewater treatment. Due to the discrepancy of their chemical molecular structures, it can be inferred the utilizing pathways of these two carbon sources by microorganisms are different, which may affect the nitrogen metabolism processes and the denitrification efficacies. However, limited comparative research focus on the nitrate removal performance and metabolic pathway using these two carbon sources have been reported. Shen et al. [9] reported that nitrate removal efficiency was improved by 26.3% using ethanol as the carbon source compared with that of starch/poly(lactic acid) (SPLA9). Ge et al. [11] found that carbon sources significantly impacted nitrate removal and observed evident nitrite accumulation at low C/N ratios ($C/N \leq 1.0$). Consequently, it is essential to optimize carbon source selection and the C/N ratio to obtain the desired nitrate removal efficiency for biological denitrification.

Some novel bioprocesses have achieved favorable performance. Xu et al. [12] used a lab-scale pack-bed bioreactor to treat nitrate-rich wastewater and results showed that 92% and 79% of nitrate could be removed at a C/N ratio of 3.6 for glucose and sodium acetate systems, respectively. Hao et al. [13] employed a three-dimensional biofilm electrode reactor (3D-BER) for denitrification of simulated municipal wastewater treatment plant effluent and a nitrate removal of 98.3% was obtained at a C/N ratio of 3.0 and a hydraulic retention time (HRT) of 7 h. Moreover, some researchers utilized membrane bioreactors for the cultivation of denitrifying bacteria to enhance nitrate removal [14]. Compared with other bioprocesses, membrane bioreactors can achieve complete retention of denitrifying bacteria, thereby achieving higher process efficiency and lower sludge yield, which has advantages in enhancing biological nitrate removal [15].

However, fouling behavior will inevitably occur when a membrane bioreactor is utilized to enhance biological nitrate removal. For anoxic-membrane bioreactors (AnoMBRs)/denitrifying membrane bioreactors (DNMBRs), membrane fouling behavior characteristics, and mechanisms are significantly different from that of aerobic or anaerobic membrane bioreactors. This is attributed to different biological metabolic pathways of the microorganisms resulting from

different redox environments, thereby affecting sludge filterability [16]. During denitrification, microorganisms are more prone to generate metabolic activity. Denitrification can induce variation in the physicochemical/biochemical properties of the activated sludge, such as for the disintegrated floc and particle size, that can directly impact the membrane fouling behavior. Therefore, given that the discrepancy of the metabolic pathways using acetic acid and ethanol as carbon sources, different sludge characteristics can be induced, thereby resulting in diverse sludge filterability and biofouling potentials. To date, the systemic effects of the carbon source (sodium acetate and ethanol) and C/N ratio on membrane fouling behaviors in DNMBRs have rarely been reported. McAdam et al. [16] studied the effects of different substrates on the fouling behavior characteristics for an anoxic process and showed that the sludge floc has strong shear resistance and good filterability when ethanol was used as the carbon source, but the C/N ratio was not explored. Hao et al. [17] reported that the C/N ratio was an important factor controlling the membrane fouling behavior in an aerobic membrane bioreactor (MBR). Given the differences between aerobic and anoxic MBR processes, it can be speculated that the C/N ratio will have a significant influence on denitrification, thereby the membrane fouling behavior and can be taken as a controlling parameter to optimize a DNMBR.

In this study, sodium acetate and ethanol were employed as the external carbon sources to enhance denitrification in a DNMBR and the impacts of the carbon source and C/N ratio on the process performance were evaluated. Also, the membrane fouling behavior characteristics were investigated, and the changes in physicochemical/biochemical properties of the activated sludge analyzed. This study provides theoretical guidance and technical support for the improvement of biological denitrification and the sustainable operation of a DNMBR.

2. Materials and methods

2.1. Experimental set-up and operational conditions

The bench-scale DNMBR plant (Fig. 1a) comprised a rectangular bioreactor (total volume 58 L), an anoxic tank (65.5% of the total volume) with a mechanical mixer, followed by a membrane tank (34.5%) with one hollow fiber membrane (polyvinylidene fluoride; pore size: 0.04 μm ; surface area: 0.4 m^2 , Hangzhou Mina, China). A pH/DO/oxidation reduction potential (ORP) sensor (WTW Multi 3420i, Germany) was fitted to monitor the pH/DO/ORP levels in the anoxic membrane tank. The temperature was maintained at 20°C–23°C by a heater. The plant was provided with a programmable logic controller (PLC) and a data acquisition system that controlled the flows of all the streams. The membrane was operated at a constant flux of 18 $\text{L}/(\text{m}^2 \text{ h})$, with an intermittent backflushing (9 min suction and 1 min backflushing). Wastewater was pumped from the storage tank to the elevated tank, followed by the anoxic tank, the membrane tank, and finally pumped out through the membrane element. The hydraulic backflushing was demonstrated through the backflushing pump using the membrane permeate from the effluent tank at a flux of 22 $\text{L}/(\text{m}^2 \text{ h})$. The

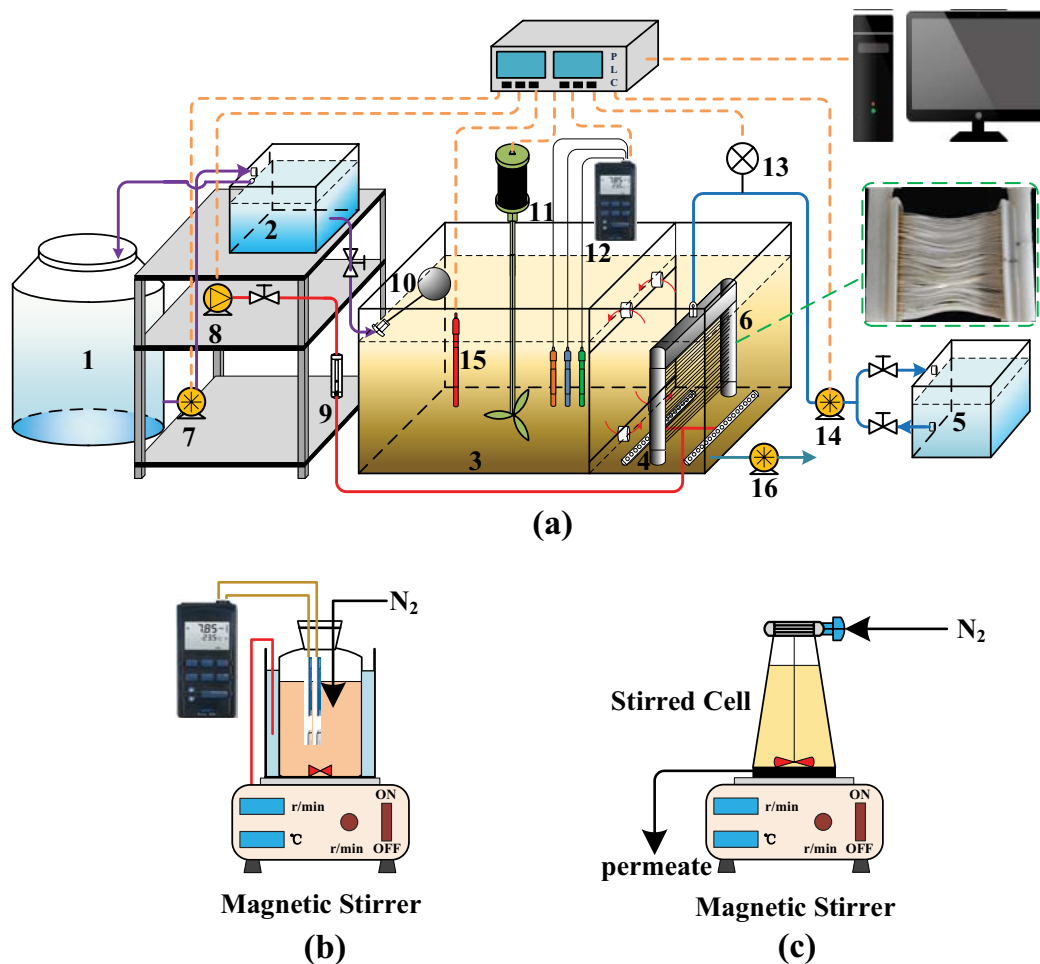


Fig. 1. Schematic diagram of (a) the DNMBR process, (b) the sequencing batch reactor, and (c) the stirred batch cell system.

membrane surface was air-scoured intermittently (10 s on, 10 s off) using coarse-bubble aerators, placed 100 mm below the membrane element channels, operating at an overall specific aeration demand (SAD_m) of $0.05 \text{ Nm}^3/(\text{m}^2 \text{ h})$. The DO concentration in the biological tank was kept at $0.2\text{--}0.5 \text{ mg/L}$ during the entire operation. The HRT was 8.0 h and a target sludge retention time (SRT) of 20 d was maintained through direct discharge of waste sludge from the membrane tank. The mixed liquor suspended solids (MLSS) concentration in the membrane tank was maintained at approximately $3,500 \text{ mg/L}$. The fouled membrane element was taken out from the aerobic tank, flushed with pure water, and soaked in NaClO solution (0.5%) for 24 h, to recover the membrane permeability at the end of each cycle.

2.2. Characteristics of feeding wastewater and inoculated sludge

Synthetic wastewater was used as the substrate. The nitrate and organic matter originated from KNO_3 and sodium acetate or ethanol, respectively. The C/N ratio was defined as the chemical oxygen demand (COD)/ NO_3^- -N ratio in the influent. The influent concentrations of nitrate and organic carbon were regulated according to the requirements of the experiment, as detailed in Table 1. The other

components included NaHCO_3 (1.0–1.25 g/L), KH_2PO_4 (0.025 g/L), $\text{MgSO}_4 \cdot 7\text{H}_2\text{O}$ (0.2 g/L), $\text{CaCl}_2 \cdot 2\text{H}_2\text{O}$ (0.3 g/L), and FeSO_4 (0.006 g/L) trace element solution I (1 ml/L), and a trace element solution II (1 ml/L). Trace element solution I contained ethylene diamine tetraacetic acid (EDTA) (5.0 g/L) and $\text{FeSO}_4 \cdot 7\text{H}_2\text{O}$ (5.0 mg/L). The trace element solution II contained EDTA (15.0 g/L), $\text{ZnSO}_4 \cdot 7\text{H}_2\text{O}$ (0.43 g/L), $\text{CoCl}_2 \cdot 6\text{H}_2\text{O}$ (0.24 g/L), $\text{MnCl}_2 \cdot 4\text{H}_2\text{O}$ (0.99 g/L), $\text{CuSO}_4 \cdot 5\text{H}_2\text{O}$ (0.25 g/L), $\text{Na}_2\text{MoO}_4 \cdot 2\text{H}_2\text{O}$ (0.22 g/L), $\text{NiCl}_2 \cdot 6\text{H}_2\text{O}$ (0.19 g/L), $\text{Na}_2\text{SeO}_4 \cdot 10\text{H}_2\text{O}$ (0.21 g/L), and H_3BO_3 (0.014 g/L). The inoculated sludge was taken from the east wastewater treatment plant of Handan, Hebei Province, which employs a T-type oxidized ditch process, achieving satisfactory biological nitrogen removal. After one week of sludge acclimation, a stable performance was achieved and experiments commenced according to the influent setting requirements.

2.3. Analytical methods

2.3.1. Wastewater and sludge analysis

COD, NH_4^+ -N, NO_3^- -N, NO_2^- -N, TN, and MLSS were measured according to standard methods [18]. The pH, DO, ORP, and temperatures were determined by a multiparameter sensor (WTW Multi 3420i, Germany). The sludge

Table 1
Influent characteristics during different operational phases

	Sodium acetate			Ethanol		
	I	II	III	IV	V	VI
Times (d)	0–15	16–30	31–45	46–60	61–75	76–90
pH	7.57	7.65	7.63	7.58	7.62	7.69
COD (mg/L)	31.8	97.1	153.2	33.2	98.9	164.6
NO ₃ ⁻ -N (mg/L)	31.9	32.5	30.7	33.6	32.9	32.9
C/N ratio	1.0	3.0	5.0	1.0	3.0	5.0
CLR (kg/m ³ d)	0.10	0.29	0.46	0.10	0.30	0.49
NLR (kg/m ³ d)	0.09	0.10	0.09	0.10	0.10	0.10

Average values of the experimental data are presented in the table.

viscosity was measured using a viscometer (Brookfield DV2T, USA) with a V71 rotor at a rotating speed of 50 rpm; the capillary suction time (CST) was measured using a portable CST instrument (Hangzhou Dealfine DFC-10A, China); the particle size distribution of the activated sludge from the membrane tank was measured using a Mastersizer counter (Marlvern 2000, UK).

Total nitrogen (TN) was calculated by the sum of ammonia, nitrite, and nitrate. Nitrogen removal efficiency (NRE), nitrogen loading rate (NLR), nitrogen removal rate (NRR), COD removal efficiency (CRE), COD loading rate (CLR), and COD removal rate (CRR) were calculated with the following equations:

$$\text{NO}_3^- - \text{N}_{\text{RE}} = \frac{\text{NO}_3^- - \text{N}_{\text{Inf}} - \text{NO}_3^- - \text{N}_{\text{Eff}}}{\text{NO}_3^- - \text{N}_{\text{Inf}}} \times 100\% \quad (3)$$

$$\text{NRE} = \frac{\text{TN}_{\text{Inf}} - \text{TN}_{\text{Eff}}}{\text{TN}_{\text{Inf}}} \times 100\% \quad (4)$$

$$\text{NLR} = \frac{\text{TN}_{\text{Inf}}}{\text{HRT}} \quad (5)$$

$$\text{NRR} = \frac{\text{TN}_{\text{Inf}} - \text{TN}_{\text{Eff}}}{\text{HRT}} \quad (6)$$

$$\text{CRE} = \frac{\text{COD}_{\text{Inf}} - \text{COD}_{\text{Eff}}}{\text{COD}_{\text{Inf}}} \times 100\% \quad (7)$$

$$\text{CLR} = \frac{\text{COD}_{\text{Inf}}}{\text{HRT}} \quad (8)$$

$$\text{CRR} = \frac{\text{COD}_{\text{Inf}} - \text{COD}_{\text{Eff}}}{\text{HRT}} \quad (9)$$

where NO₃⁻-N_{Inf}, TN_{Inf} and COD_{Inf} are the concentrations of NO₃⁻-N, TN, and COD in the influent, respectively; NO₃⁻-N_{Eff}, TN_{Eff} and COD_{Eff} are the concentrations of NO₃⁻-N, TN, and COD in the effluent, respectively; HRT is the hydraulic retention time (d).

2.3.2. Analysis of the activities of the functional bacteria

Sequencing batch tests were conducted with 250 mL serum flasks, as shown in Fig. 1b. First, the activated sludge was collected from the anoxic tank and washed using deionized water for residue removal. Then, the serum flask, to which 100 mL sludge and 150 mL of a prepared matrix (as detailed in Table 2) were added, was placed on a magnetic stirrer (500 rpm) with high purity nitrogen blown in to remove the dissolved oxygen when the activity tests of denitrification were performed. The control temperature was maintained at 25°C ± 1°C. The NO₃⁻-N, NO₂⁻-N, and NH₄⁺-N concentrations in the supernatants of the serum flasks were determined. The DNB activity was characterized by evaluating specific degradation rates of NO₃⁻-N (SDR_{NO₃⁻-N}, mg N/(mg MLSS d)) and NO₂⁻-N (SDR_{NO₂⁻-N}, mg N/(mg MLSS d)), respectively. The specific accumulation rate of NO₂⁻-N (SAR_{NO₂⁻-N}, mg N/(mg MLSS d)) and ammonia (SAR_{NH₄⁺-N}, mg N/(mg MLSS d)) were also determined.

2.3.3. Evaluation of membrane fouling rate and fouling resistance

The trans-membrane pressure (TMP, kPa) data was calibrated by the standard temperature (θ, 20°C), as defined in Eq. (10):

$$\text{TMP} = \text{TMP}_0 e^{0.023(\theta-20)} \quad (10)$$

The membrane fouling rate (Fr, L/(m² h² kPa)) was defined as the permeability decline rate and was calculated according to Eq. (11):

$$\text{Fr} = \frac{J_e}{\text{TMP}_e \cdot t} - \frac{J_i}{\text{TMP}_i \cdot t} \quad (11)$$

where J_i and TMP_i are the membrane permeation flux and e the trans-membrane pressure at the beginning of each running cycle; J_e and TMP_e are the membrane permeation flux and trans-membrane pressure at the end of each running cycle; and t is the duration of each running cycle.

Membrane resistance was analyzed based on Darcy's law, as shown in Eq. (12):

Table 2
Substrates of the sequencing batch tests

Functional bacteria	DNB _{NO₂-N}	DNB _{NO₃-N}
NH ₄ ⁺ -N (mg/L)	0	0
NO ₂ -N (mg/L)	0	30
NO ₃ -N (mg/L)	30	0
COD (mg/L)	30–150	30–150

$$J = \frac{\text{TMP}}{\mu R_t} = \frac{\text{TMP}}{\mu (R_f + R_m)} = \frac{\text{TMP}}{\mu (R_c + R_p + R_m)} \quad (12)$$

where R_t is the total hydraulic resistance, R_m is the membrane resistance, R_c is the cake layer resistance, R_p is the pore-blocking resistance, μ is the dynamic viscosity of the permeate, and J is the membrane permeate flux. Each resistance was determined according to the following experimental procedures: R_m was computed by measuring the flux and TMP of tap water using a new hollow fiber membrane; R_t was evaluated from the final data after biomass ultrafiltration; the cake layer on the membrane surface was wiped with a sponge and simultaneously flushed by tap water, and the membrane was then submerged in tap water to obtain flux and TMP data to calculate $R_m + R_p$. Then R_c and R_p were determined by subtraction according to Eq. (11).

2.3.4. Extraction and analysis of extracellular polymeric substances and soluble microbial production

The extraction of extracellular polymeric substances (EPS) and soluble microbial production (SMP) was based on a heating method [19]: 50 mL sludge mixture was taken and centrifuged at $5,000 \times g$ for 5 min, at 4°C. Next, SMP was obtained by filtering the supernatant through a 0.45 μm membrane filter. After that, the sludge pellets were resuspended to their original volume, using a buffer consisting of 2 mM Na₃PO₄, 4 mM NaH₂PO₄, 9 mM NaCl, and 1 mM KCl, at pH 7.0. Subsequently, the sludge suspension was heated in an oven for 2.0 h at 105°C and was then centrifuged at $12,000 \times g$ for 15 min at 4°C to remove remaining floc components. EPS was obtained by filtering the supernatant through a 0.45 μm membrane filter. The EPS and SMP were normalized as the sum of carbohydrates and proteins, whose concentrations were determined using the modified Bradford method with bovine serum albumin as the standard and the anthrone–sulfuric acid colorimetric method with glucose as the standard, respectively [20]. The molecular weight of EPS and SMP were fractionated by a series of ultrafiltration membranes (1,10, and 100 kDa, Millipore, USA) using a stirred cell at a constant pressure of 30 kPa (Fig. 1c).

2.3.5. Membrane foulant extraction and FT-IR analysis

The fouled membrane element was taken out from the membrane tank and flushed with pure water at the end of each running cycle. Approximately 300 mL washed liquid was taken and placed in a dryer at 105°C for 24 h, to obtain dry foulants. KBr pellets containing 0.5% (dry powder) of

the sample were prepared, then the major functional groups of foulants samples were characterized using a Fourier transform infrared spectrometer (FT-IR Affinity-1, Japan). The spectrum was calculated as the average of 256 scans, with the wave number ranging from 4,000 to 400 cm^{-1} , at a resolution of 4 cm^{-1} , and the detected data were processed with OriginPro 8.0.

3. Results and discussion

3.1. Process performance

3.1.1. Different carbon sources and C/N ratios on the denitrification performance

The effects of different carbon sources and C/N ratios on the denitrification performance are depicted in Figs. 2a and b. It can be seen that similar nitrate removal trends were exhibited in sodium acetate and ethanol systems. The average nitrate removal efficiency was only 28.50%, with an effluent concentration of 22.80 mg/L at a C/N ratio of 1.0 (phase I) in the sodium acetate system. This was attributed to the insufficient carbon source as electron donors for heterotrophic denitrification [21]. Meanwhile, even lower nitrate removal (23.58%) was obtained in the ethanol system (phase IV). However, similar COD consumption (30.34–31.73 mg/L) and CREs (95.5%–95.6%) were achieved in both systems during phases I and IV. This suggests that denitrifiers could promptly adapt to the two carbon sources and were able to carry them directly for denitrification metabolism. Additionally, the average nitrite concentration was 0.78 mg/L in both systems, indicating inconspicuous nitrite accumulation that may be the result of the relatively long HRT during the operations [22].

With the increase in the C/N ratio to 3.0 (phases II and V), the nitrate removal efficiency reached 96.10% and 95.58% stably after 2 d adaptation, with nitrate concentration sharply decreasing to 1.26 and 1.46 mg/L in the sodium acetate and ethanol systems, respectively. The average COD consumption rose to approximately 93.00 mg/L in both systems. Stable NRE of 95.64%, NRR of 0.09 $\text{kg}/(\text{m}^3 \text{d})$, and CRR of 0.28 $\text{kg}/(\text{m}^3 \text{d})$ were obtained at C/N ratio of 3.0% and 25.89%, 0.03 $\text{kg}/(\text{m}^3 \text{d})$, and 0.09 $\text{kg}/(\text{m}^3 \text{d})$ at C/N ratio of 1.0 in the sodium acetate system. For the ethanol system, the NRE, NRR, and CRR increased by 76.04%, 0.07 $\text{kg}/(\text{m}^3 \text{d})$, and 0.18 $\text{kg}/(\text{m}^3 \text{d})$ at C/N ratio of 3.0 from those at the C/N ratio of 1.0. Moreover, in the sodium acetate system, pH increased from 8.08 (effluent) at C/N ratio of 1.0–8.42 (effluent) at C/N ratio of 3.0 under the condition of influent pH in the range of 7.57–7.65, which was similar as the pH trends (from 7.99 to 8.49) in the ethanol denitrification system. Normally, the pH value increase after the denitrification bioreaction due to the alkalinity production, which make it as an denitrification indicator. A higher pH value in the effluent usually indicates a more thorough denitrification performance to achieve a relative higher NRE. The increased pH values (effluent) at a C/N ratio of 3.0 in both systems proved that the denitrification processes were demonstrated more completely with the supplements of electron donors. These results also strongly suggest that the increase in the C/N ratio could significantly improve nitrate removal in a DNMBR. According to the process bioreaction, the theoretical amount of COD needed for complete denitrification

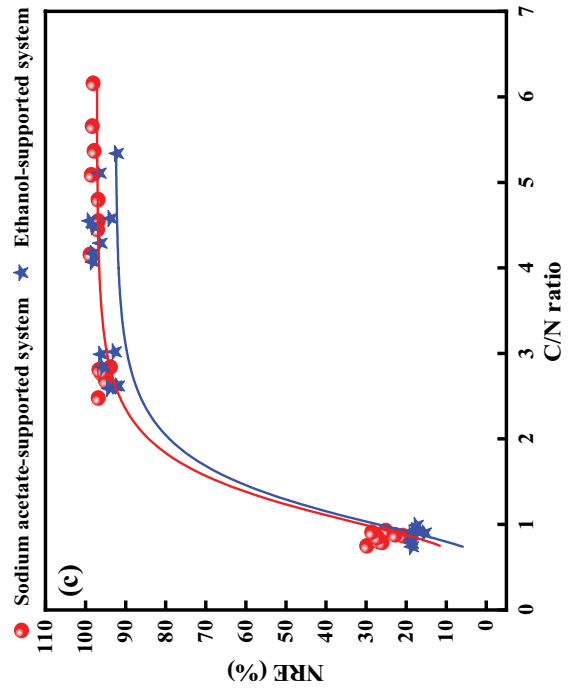
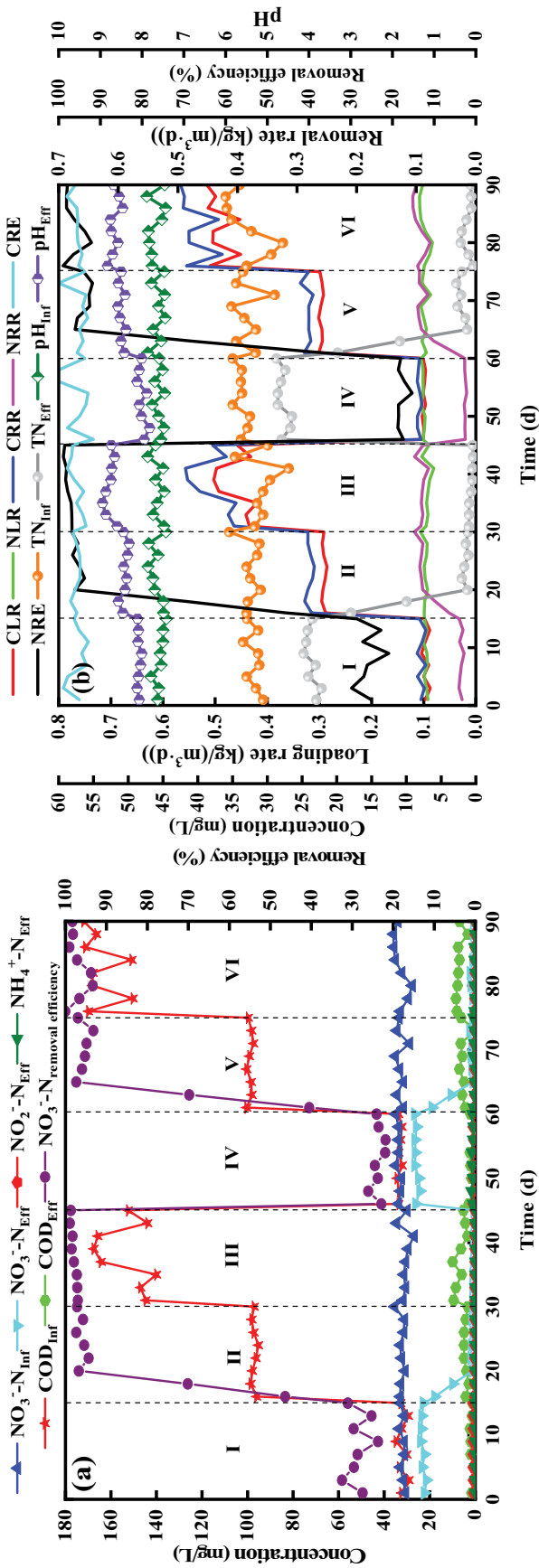


Fig. 2. Changes in (a) $\text{NO}_3^- \text{N}_{\text{Inf}}$, $\text{NO}_3^- \text{N}_{\text{Eff}}$, $\text{NO}_2^- \text{N}_{\text{Eff}}$, $\text{NH}_4^+ \text{N}_{\text{Eff}}$, COD_{Inf} , COD_{Eff} and $\text{NO}_3^- \text{N}$ removal, (b) total nitrogen removal, NLR, NRR, CLR, CRR, CRE, pH_{Inf} and pH_{Eff} during different operational phases, and (c) correlations of the C/N ratio with NREs in the sodium acetate and ethanol systems.

is 2.86 g COD/g NO₃-N. The actual COD consumption for the denitrification was 3.30 and 3.34 g COD/g NO₃-N in the sodium acetate and ethanol systems, respectively, which was higher than the theoretical value. This may result from the carbon oxidation process by other heterotrophic bacteria induced by dissolved oxygen (DO) in the influent.

With a further increase in the C/N ratio to 5.0 (phases III and VI), there was only a slight increment of 1.83% and 2.16% in nitrate removal efficiency and NRE than those at a C/N ratio of 3.0 in the sodium acetate system. For the ethanol system, a similar increasing trend was obtained with an increase of 1.45% and 2.66% for the nitrate removal efficiency and NRE, respectively. The pH value finally rose to 8.77 and 8.67 in the sodium acetate and ethanol systems. These results suggested with an increase of 2.0 in the C/N ratio there was a slight enhancement of nitrate removal with a CRR of 0.44 and 0.47 kg/(m³·d) obtained in sodium acetate and ethanol systems, respectively. Furthermore, the possible critical transition was revealed for nitrate removal at a C/N ratio of 3.0 in both systems, which was further shown by correlation between the C/N ratio and NRE, as shown in Fig. 2c. An evident turning point was observed at the C/N ratio of 3.0, indicating the significant boundary of the NRE increment with the increase in the C/N ratios. Lognormal fittings can also be employed for the NRE prediction model (the formulas expressed as Eqs. (13) and (14)) for the expected increase in the C/N ratio.

In summary, the carbon source and C/N ratio were two significant affecting factors for the nitrate removal with the latter outweighing the former. Generally, it is speculated that complete denitrification can be achieved without nitrite and ammonia accumulation. Notably, effluent ammonia concentration (0.01–0.05 mg/L) was lower in the sodium acetate than that (0.16–1.18 mg/L) in the ethanol supported system, which can be attributed to the variant functional genes induced by the different carbon sources resulting in the discrepancies of nitrate removal pathways [12]. Srinandan et al. [23] reported that ammonia accumulates through the dissimilatory nitrate-to-ammonia (DNRA) process by employing ethanol and glucose as electron donors. Therefore, it is vital to choose the appropriate carbon source to constrain the DNRA pathway to achieve better nitrogen removal performance.

$$Y = 92.99 + \frac{-94.6}{\sqrt{2\pi \times 0.65X}} e^{-\frac{\left[\ln \frac{X}{0.93}\right]^2}{0.85}} R^2 = 0.969 \quad (13)$$

$$Y = 88.88 + \frac{-95.24}{\sqrt{2\pi \times 0.62X}} e^{-\frac{\left[\ln \frac{X}{0.88}\right]^2}{0.77}} R^2 = 0.974 \quad (14)$$

3.1.2. Functional bacteria activity and denitrification pathways

The functional bacteria activities were further assessed to explain the variations in the process performance during different operational phases, as presented in Fig. 3a. SDR_{NO₃-N} increased from 0.041 mg/(mg MLSS d) to 0.226 mg/

(mg MLSS d) with the C/N ratio increasing from 1.0 to 5.0. In the ethanol system, a similar increasing trend of SDR_{NO₃-N} of 0.032–0.219 mg/(mg MLSS d) was observed, indicating that the increase in the electron donors promoted the functional bacteria activities in the DNMBR. Meanwhile, SDR_{NO₃-N} was always higher in the sodium acetate systems under various C/N ratios, which was in agreement with the nitrate removal efficiency during different operational phases. This was attributed to the shorter metabolic pathway using sodium acetate as the carbon source, in which the sodium acetate could directly enter the tricarboxylic acid cycle by combining with coenzyme A to supply electrons and energy [24]. However, for methanol, it had to be converted into low-weight molecular organic acids, such as acetic acid, before being utilized by the denitrifiers. Thus, from the view of metabolic processes, sodium acetate showed its inherent advantage for the enhancement of nitrate removal. Furthermore, SAR_{NO₂-N} of 0.014 and 0.013 mg/(mg MLSS d) were observed in the sodium acetate and ethanol systems at the C/N ratio of 1.0, respectively. SAR_{NO₂-N} decreased with the C/N ratio, eventually to 0.001 mg/(mg MLSS d) in both systems, revealing the nitrite accumulation during denitrification was more dependent on the C/N ratio. SDR_{NO₂-N} values were slightly larger than those of SDR_{NO₃-N} at a low C/N ratio of 1.0, whereas this trend vanished with higher C/N ratios. This could be explained by the temporary repression of nitrite reductase from over-competition with nitrate reductase for electrons at low C/N ratios [25]. The nitrite accumulation resulting from the inhibited nitrite reduction rate during the denitrification process can be eliminated if enough electron donors are offered. The positive linear correlations between the C/N ratio and SDR_{NO₃-N} and SDR_{NO₂-N} are illustrated in Figs. 3b and c, which suggests the internal rules of C/N ratio in affecting functional bacteria activities.

Additionally, the ethanol system showed ammonia accumulations with SAR_{NH₄⁺-N} in range of 0.001–0.007 mg/(mg MLSS d), which was not seen in the sodium acetate system. This suggested the carbon source types significantly affected ammonia accumulations, possibly resulting from the differences in microbial community structure and denitrification functional genes [26], which needed further study. It seemed that ethanol would induce DNRA corresponding to the higher effluent NH₄⁺-N concentration, which is consistent with Yang et al. [27]. Xu et al. [12] also reported that higher proportions of functional genes (*NirB*, *NirD*, *NrfH*, and *NfrA*) were the main causes of ammonia accumulation in the DNRA.

In summary, the carbon source and C/N ratio had a great influence on functional bacteria activity and denitrification pathways. Complete denitrification was observed and results suggest that immediate or dissimilatory products are minimized to achieve the higher nitrogen removal levels.

3.2. Membrane fouling

3.2.1. Membrane fouling behaviors

The evolution of TMP and flux during different operational phases is shown in Fig. 4a. The membrane module was taken out of the membrane tank to demonstrate the off-line chemical cleaning to recover the membrane permeability

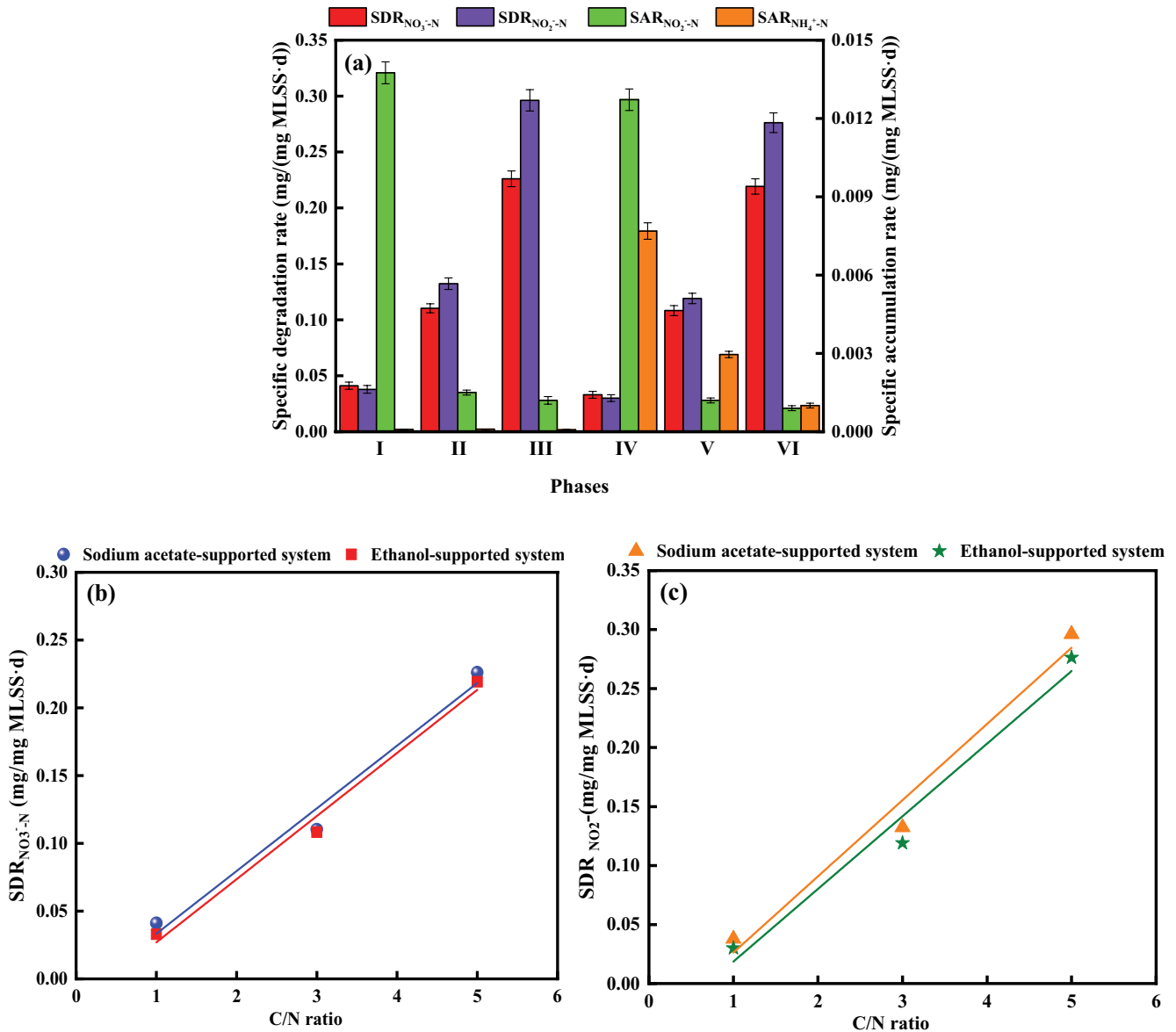


Fig. 3. (a) Activities of the functional bacteria during different operational phases, correlations of (b) SDR_{NO₃-N} and (c) SDR_{NO₂-N} in the sodium acetate and ethanol systems.

when the DNMBR reached the TMP limit (50 kPa) or the ending point of the operational period. It was observed that the membrane fouling rate increased with the C/N ratio for both sodium acetate and ethanol systems. The membrane fouling rate was higher (0.23–0.55 L/(m² h² kPa)) in the ethanol system than that (0.14–0.39 L/(m² h² kPa)) of the sodium acetate system. Typical apparent features of membrane fouling when reaching the TMP limit are presented in Fig. 5 distinct membrane fouling behaviors during different operational phases. These discrepancies could be the result of the variations in the distributions of membrane fouling resistances, as detailed in Fig. 4b. The deep pore-blocking played a dominant role (49.6%–71.9%) in the membrane fouling resistance in the sodium acetate system. Conversely, the contribution ratio of bio-cake (20.2%–75.5%) in the ethanol system was higher than that of the sodium

acetate system and was the leading factor for the membrane fouling behavior in phase VI. This revealed that there was a significant difference in the membrane fouling mechanisms between sodium acetate and ethanol systems and possible reasons are suggested in the following sections.

3.2.2. Particle size distribution of activated sludge

The particle size distributions of the activated sludge from the membrane tank during different operational phases are presented in Fig. 6. It is well-known that particle size is a key parameter affecting the membrane fouling behaviors in various MBR processes [28,29]. Normally, the smaller sludge floc would easily adhere to the membrane surface and combine with the biopolymers to form a dense cake layer, thus decreasing the porosity and permeability of the membrane

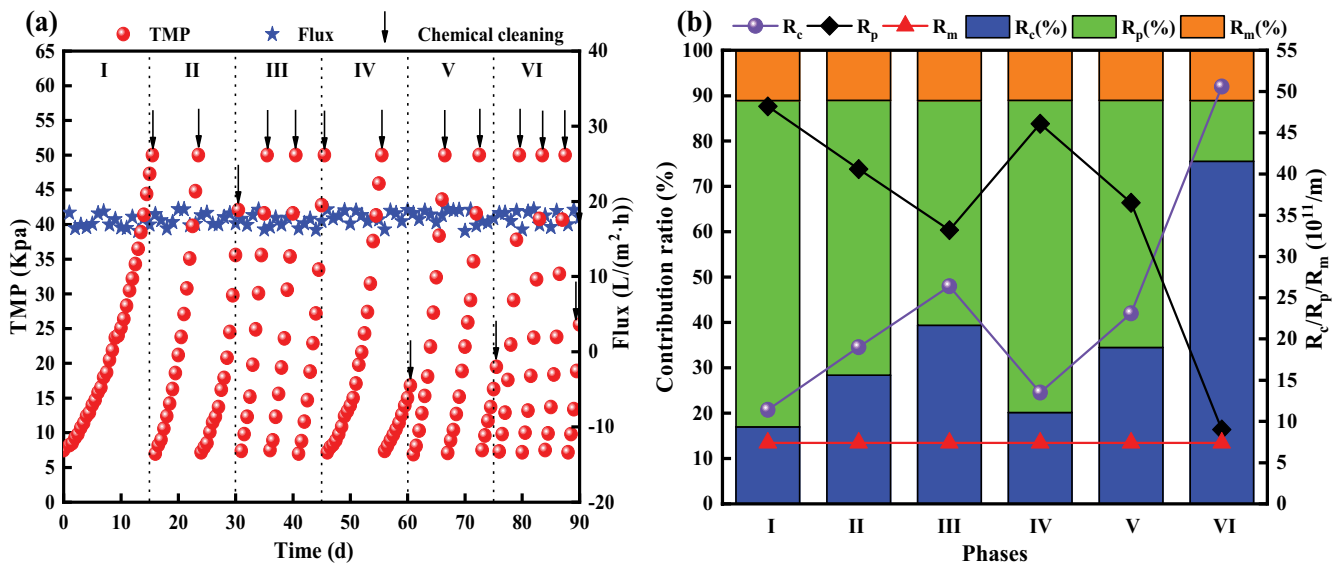


Fig. 4. (a) Evolution of TMP and Flux and (b) distribution of membrane filtration resistance during different operational phases.

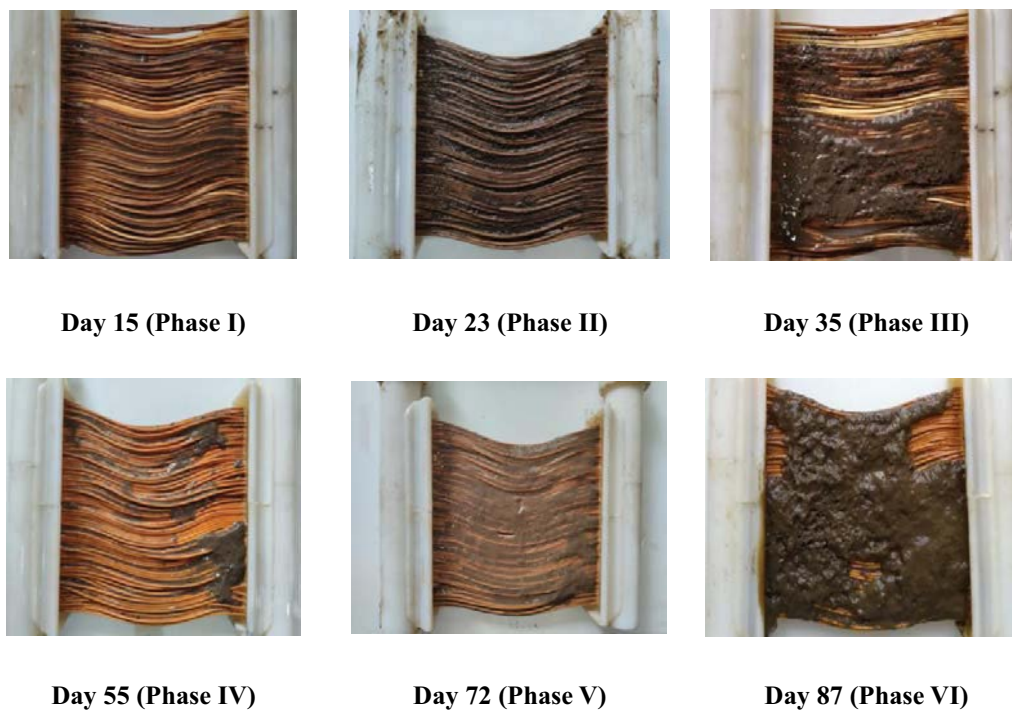


Fig. 5. Features of the membrane module reaching the TMP limit during different operational phases.

module [30]. The floc size was influenced by the different carbon sources and C/N ratio-induced denitrification processes. The average particle size decreased from 62.3 μm at a C/N ratio of 1.0–51.5 μm at a C/N ratio of 5.0 in the sodium acetate system, which was attributed to the floc disintegration effects during the enhancement of nitrate removal. Wang et al. [31] reported that the increased shear forces induced by dinitrogen productions during denitrification lead to sludge disintegration, thus producing larger fractions of smaller particles in mixed culture. Similarly, the

ethanol system showed a decreasing trend of average particle size from 53.9 to 49.6 μm at the corresponding C/N ratios. It should be noted that the average floc size was larger in the sodium acetate system than in the ethanol system, perhaps because different carbon sources induced the microbial community structure shift, which exhibited their unique flocculation and anti-disintegration capabilities when exposed to shear stress. Thus, the variations in the particle size distributions were a combined consequence of the demonstrated shear forces and sludge anti-disintegration behaviors.

3.2.3. EPS and SMP production

The large differences in metabolic production associated with the content and composition of EPS and SMP were observed during different operational phases, as is illustrated in Figs. 7a and b. It has been generally considered that EPS and SMP act as the fouling indicators in membrane bioreactor processes, where EPS plays a vital role in the formation of the cake layer, and SMP is regarded as the main cause for the deep pore-blocking [32]. Interestingly, the EPS content was lower in the sodium acetate system than that of the ethanol system, whereas the SMP content was

higher in the former. These findings are possibly attributed to the difference in the metabolic pathways during denitrification employing different carbon sources. More specifically, the EPS content increased from 22.13 to 30.62 mg/g in the sodium acetate system, much lower than that of the ethanol system (31.35–32.72 mg/g). The carbohydrate fraction of EPS (EPS_c)/the protein fraction of EPS (EPS_p) ratio decreased from 1.18 in phase I to 0.87 in phase III, which indicated that the hydrophobic EPS_p played an increasingly important role in bio-cake formation in the sodium acetate system. However, the EPS_c content was lower than that of EPS_p and the EPS_c/EPS_p ratio was relatively stable (in the range of 0.70–0.74) in phase IV–VI, which suggested the EPS_p was the main contributor to the biocake resistance throughout. Comparatively, SMP content increased from 104.1 to 145.5 mg/L, with a much higher the carbohydrate fraction of SMP (SMP_c) (62.97–83.1 mg/L) in phases I–III. These results revealed SMP_c was of great importance in contributing to the pore-blocking despite the SMP_c/the protein fraction of SMP (SMP_p) ratio decreasing from 1.53 to 1.30 [33]. In contrast, SMP_p content was relatively stable (66.5–77.8 mg/L) with an SMP_c/SMP_p ratio increasing 0.32–0.51 from phase IV to VI.

Also, the bimodal molecular weight distributions of EPS and SMP were observed during different operational phases and were similar to other experimental findings [34]. The sodium acetate and ethanol systems showed similar molecular weight distributions for EPS and SMP, of which the fractions of EPS_{>100 kDa}, SMP_{>100 kDa}, EPS_{<1 kDa}, and SMP_{<1 kDa} were approximately 38.9%, 30%, 42.0%, and 30.1%, respectively. The SMP_c with a large molecular weight, would accumulated in the deep pores, thereby inducing the gel layer formation on the membrane surface [35], whereas the low molecular fractions could permeate through membrane pores as the organic matter in the effluent. Thus, combined with the results above, the SMP_{>100 kDa} fraction was

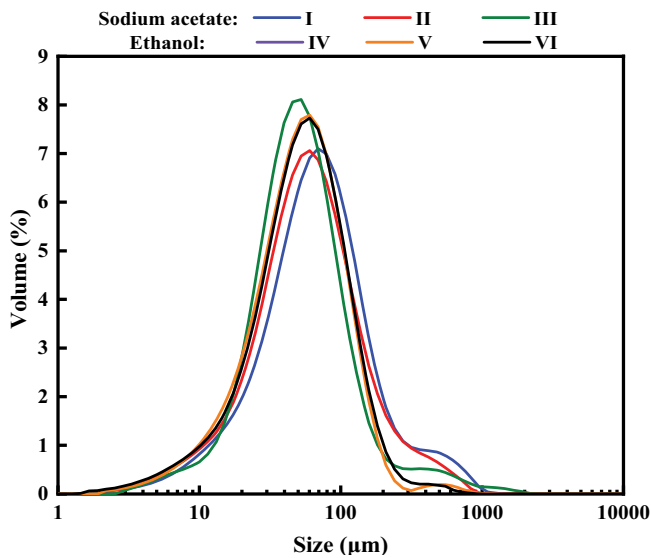


Fig. 6. Particle size distributions of the activated sludge during different operational phases.

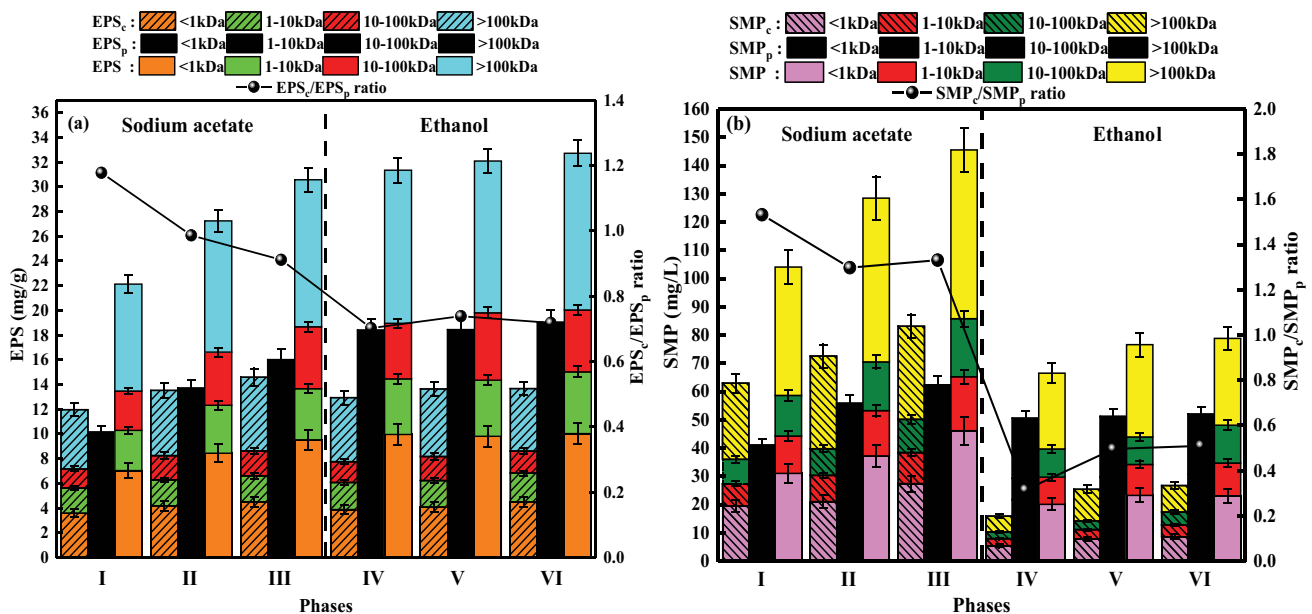


Fig. 7. Variation in the content and composition of (a) EPS and (b) SMP during different operational phases.

considered as the key pore-blocker for membrane fouling behavior in the sodium acetate system. Zhang et al. [36] also found that the $SMP_{>100\text{ kDa}}$ fraction aggravated the membrane fouling behavior through an adherence effect to block the membrane pores. Similarly, the large molecular weight fraction of EPS (especially EPS_p due to its predominant role in the EPS composition) was prone to attach on the membrane surface, which could combine with smaller flocs to form an evident biocake. It can be deduced that in an ethanol-supported system, $EPS_{p>100\text{ kDa}}$ exerted a marked impact on cake layer formation.

3.2.4. Variations in sludge viscosity and capillary suction time

To evaluate the impacts of carbon source and C/N ratio on the sludge filterability, the sludge rheology and dewaterability were further assessed with references to sludge viscosity and CST, as shown in Fig. 8. Normally, lower sludge viscosity and CST would improve the sludge filterability as well as membrane permeability. The sludge viscosity is influenced by various factors, such as temperature, microbial metabolic productions (SMP, EPS), and floc sizes [37,38]. It was reported that higher microbial production and smaller particle size would result in higher sludge viscosity, thereby inducing the adherence of sludge particles on a membrane surface [39]. Similarly, higher CST could lead to greater separation difficulty of water from the activated sludge, which mainly results from the higher amount of EPS production [40]. It was observed that the sludge viscosity (20.78–21.15 mPa S) and CST (7.9–10.5 s) were lower in the sodium acetate system than those (20.82–21.34 mPa S, 8.2–11.6 s) of the ethanol system at different C/N ratios, respectively, which indicated that better sludge filterability was obtained in the former. Additionally, the best and worst sludge filterability was achieved in phase I and VI, corresponding with the observed lowest and highest fouling rates, respectively.

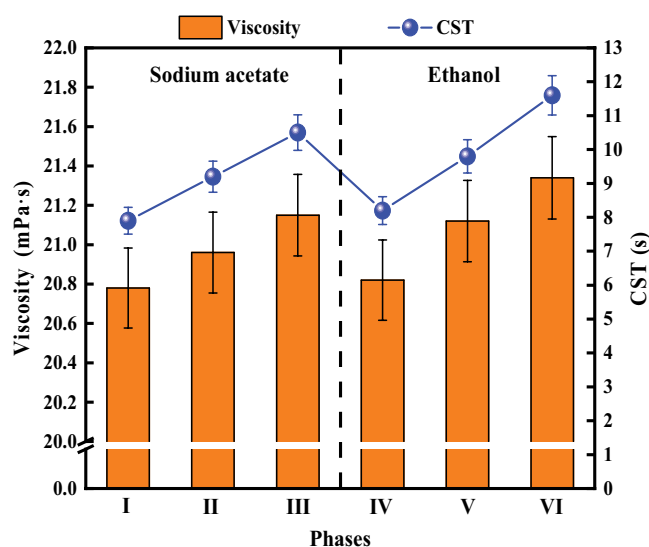


Fig. 8. Changes of viscosity and CST of the activated sludge during different operational phases.

3.2.5. FT-IR analysis of membrane foulants

The infrared spectra of the functional groups of the membrane foulants during different operational phases are illustrated in Fig. 9. Similar infrared spectral responses were obtained, indicating the similar compositions of the membrane foulants in sodium acetate and ethanol systems. There were peaks at 3,441; 2,930; 1,643; 1,415; 1,041; and 869 cm^{-1} in all infrared spectrum profiles. More specifically, the peak at 3,414 cm^{-1} was related to the O–H stretching vibration in the hydroxyl groups. The slight absorption peak at 2,939 cm^{-1} was caused by the C–H expansion vibration in alkane organic matter and polysaccharide molecules. The intensive absorption bands at 1,651 and 1,415 cm^{-1} confirmed the existence of the secondary protein structures. Also, an absorption peak could be seen at 1,041 cm^{-1} , which was associated with the C–O–C stretching vibration of carbohydrate-like substances [41,42]. However, no absorption peaks were found in the fingerprint region. These results suggest that protein-like and carbohydrate-like substances were the main contributors to the membrane foulants.

4. Conclusion

The nitrate removal and membrane fouling behavior were impacted by the different types of carbon sources and variation in C/N ratios to varying degrees in the DNMBR. Comparatively, the sodium acetate system showed a better overall nitrogen reduction, resulting from higher nitrate removal and less ammonia production. Furthermore, data suggest nitrite accumulation is minimized to achieve complete denitrification. Better sludge filterability and a lower fouling rate were obtained in the sodium acetate system, in which $SMP_{>100\text{ kDa}}$ was the main reason for the pore-blocking. For the ethanol system, the $EPS_{p>100\text{ kDa}}$ fraction combined with smaller particles and accelerated cake layer formation. The current study presented a thorough evaluation of nitrogen removal performance and provided insights into membrane

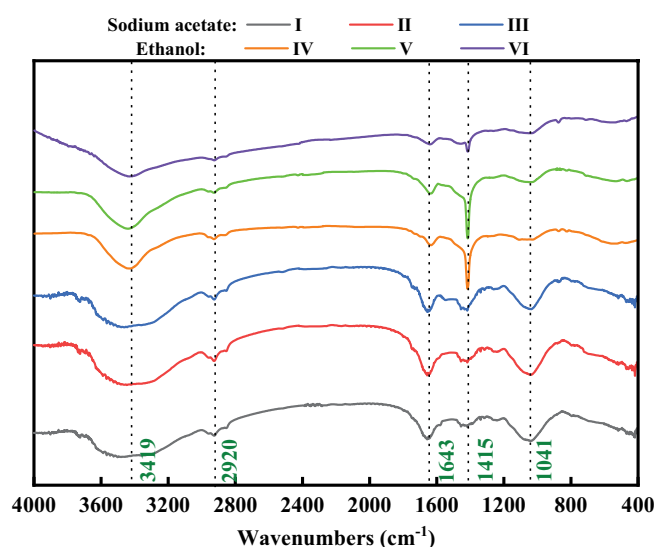


Fig. 9. FT-IR spectra of the membrane foulants during different operational phases.

fouling mechanisms using sodium acetate and ethanol as external electron donors, offering technical guidance for the optimal selection of a carbon source. Future research should be focused on the linkage between microbial community structure and metabolic production in the DNMBRs.

Acknowledgments

This work was financially supported by Hebei Provincial innovation funding project for graduate students (CXZZSS2019071), Hebei Provincial Natural Science Fund Project (E2016402017), and Project of Young Top Talents Program in Universities and Colleges of Hebei Province (BJ2019029).

References

- [1] L.Q. Wang, Y. Li, C.Y. Fan, P.F. Wang, L.H. Niu, L.F. Wang, Nitrate addition promotes the nitrogen cycling processes under the co-contaminated tetrabromobisphenol A and copper condition in river sediment, *Environ. Pollut.*, 251 (2019) 659–667.
- [2] L.E. Hanache, L. Sundermann, B. Lebeau, J. Toufaily, T. Hamieh, T.J. Daou, Surfactant-modified MFI-type nanozeolites: super-adsorbents for nitrate removal from contaminated water, *Microporous Mesoporous Mater.*, 283 (2019) 1–13.
- [3] X. Jiang, D.W. Ying, D. Ye, R.Q. Zhang, Q.B. Guo, Y.L. Wang, J.P. Jia, Electrochemical study of enhanced nitrate removal in wastewater treatment using biofilm electrode, *Bioresour. Technol.*, 252 (2018) 134–142.
- [4] F. Ruiz-Beviá, M.J. Fernandez-Torres, Effective catalytic removal of nitrates from drinking water: an unresolved problem?, *J. Cleaner Prod.*, 217 (2019) 398–408.
- [5] Y.H. Shi, G.X. Wu, N. Wei, H.Y. Hu, Denitrification and biofilm growth in a pilot-scale biofilter packed with suspended carriers for biological nitrogen removal from secondary effluent, *J. Environ. Sci.*, 32 (2015) 35–41.
- [6] L. Xie, J.R. Chen, R. Wang, Q. Zhou, Effect of carbon source and COD/NO₃-N ratio on anaerobic simultaneous denitrification and methanogenesis for high-strength wastewater treatment, *J. Biosci. Bioeng.*, 113 (2012) 759–764.
- [7] B. Hu, T. Wang, J.H. Ye, J.Q. Zhao, L.W. Yang, P. Wu, J.L. Duan, G.Q. Ye, Effects of carbon sources and operation modes on the performances of aerobic denitrification process and its microbial community shifts, *J. Environ. Manage.*, 239 (2019) 299–305.
- [8] Y.Q. Wu, K. Song, Y.H. Jiang, X.Y. Sun, L. Li, Effect of thermal hydrolysis sludge supernatant as carbon source for biological denitrification with pilot-scale two-stage anoxic/oxic process and nitrogen balance model establishment, *Biochem. Eng. J.*, 139 (2018) 132–138.
- [9] Z.Q. Shen, Y.X. Zhou, J.L. Wang, Comparison of denitrification performance and microbial diversity using starch/polyactic acid blends and ethanol as electron donor for nitrate removal, *Bioresour. Technol.*, 131 (2013) 33–39.
- [10] Z.H. Si, X.S. Song, Y.H. Wang, X. Cao, Y.F. Zhao, B.D. Wang, Y. Chen, A. Arefe, Intensified heterotrophic denitrification in constructed wetlands using four solid carbon sources: denitrification efficiency and bacterial community structure, *Bioresour. Technol.*, 267 (2018) 416–425.
- [11] S.J. Ge, Y.Z. Peng, S.Y. Wang, C.C. Lu, X. Cao, Y.P. Zhu, Nitrite accumulation under constant temperature in anoxic denitrification process: the effects of carbon sources and COD/NO₃-N, *Bioresour. Technol.*, 114 (2012) 137–143.
- [12] Z.S. Xu, X.H. Dai, X.L. Chai, Effect of different carbon sources on denitrification performance, microbial community structure and denitrification genes, *Sci. Total Environ.*, 634 (2018) 195–204.
- [13] R.X. Hao, S.M. Li, J.B. Li, C.C. Meng, Denitrification of simulated municipal wastewater treatment plant effluent using a three-dimensional biofilm-electrode reactor: operating performance and bacterial community, *Bioresour. Technol.*, 143 (2013) 178–186.
- [14] I. Ivanovic, T.O. Leiknes, Impact of denitrification on the performance of a biofilm-MBR (BF-MBR), *Desalination*, 283 (2011) 100–105.
- [15] F. Han, W. Ye, D. Wei, W.Y. Xu, B. Du, Q. Wei, Simultaneous nitrification-denitrification and membrane fouling alleviation in a submerged biofilm membrane bioreactor with coupling of sponge and biodegradable PBS carrier, *Bioresour. Technol.*, 270 (2018) 156–165.
- [16] E.J. McAdam, S.J. Judd, E. Cartmell, B. Jefferson, Influence of substrate on fouling in anoxic immersed membrane bioreactors, *Water Res.*, 41 (2007) 3859–3867.
- [17] L. Hao, S.N. Liss, B.Q. Liao, Influence of COD:N ratio on sludge properties and their role in membrane fouling of a submerged membrane bioreactor, *Water Res.*, 89 (2016) 132–141.
- [18] APHA, AWWA, and WEF, Standard Methods for the Examination of Water and Wastewater, 21st ed., American Public Health Association, American Water Works Association, Water Environment Federation, Washington, DC, 2005.
- [19] F. Fang, M.M. Yang, H. Wang, P. Yan, Y.P. Chen, J.S. Guo, Effect of high salinity in wastewater on surface properties of anammox granular sludge, *Chemosphere*, 210 (2018) 366–375.
- [20] J. Wu, H.M. Zhou, H.Z. Li, P.C. Zhang, J. Jiang, Impacts of hydrodynamic shear force on nucleation of flocculent sludge in anaerobic reactor, *Water Res.*, 43 (2009) 3029–3036.
- [21] S.Y. Zhai, M. Ji, Y.X. Zhao, S.G. Pavlostathis, Q. Zhao, Effects of salinity and COD/N on denitrification and bacterial community in dicyclictype electrode based biofilm reactor, *Chemosphere*, 192 (2018) 328–336.
- [22] J.L. Wang, Y.Z. Peng, S.Y. Wang, Y.Q. Gao, Nitrogen removal by simultaneous nitrification and denitrification via nitrite in a sequence hybrid biological reactor, *Chin. J. Chem. Eng.*, 16 (2008) 778–784.
- [23] C.S. Srinandan, G. D'souza, N. Srivastava, B.B. Nayak, A.S. Nerurkar, Carbon sources influence the nitrate removal activity, community structure and biofilm architecture, *Bioresour. Technol.*, 117 (2012) 292–299.
- [24] H. Constantin, M. Fick, Influence of C-sources on the denitrification rate of a high-nitrate concentrated industrial wastewater, *Water Res.*, 31 (1997) 583–589.
- [25] J.S. Almeida, M.A.M. Reis, M.J.T. Carrondo, Competition between nitrate and nitrite reduction in denitrification by *Pseudomonas fluorescens*, *Biotechnol. Bioeng.*, 46 (1995) 476–484.
- [26] D.T. Shu, Y.L. He, H. Yue, Q.Y. Wang, Microbial structures and community functions of anaerobic sludge in six full-scale wastewater treatment plants as revealed by 454 high-throughput pyrosequencing, *Bioresour. Technol.*, 186 (2015) 163–172.
- [27] X.P. Yang, S.M. Wang, L.X. Zhou, Effect of carbon source, C/N ratio, nitrate and dissolved oxygen concentration on nitrite and ammonium production from denitrification process by *Pseudomonas stutzeri* D6, *Bioresour. Technol.*, 104 (2012) 65–72.
- [28] Y. Satyawali, M. Balakrishnan, Effect of PAC addition on sludge properties in an MBR treating high strength wastewater, *Water Res.*, 43 (2009) 1577–1588.
- [29] H. Ozgun, J.B. Gimenez, M.E. Ersahin, Y. Tao, H. Spanjers, J.B.V. Lier, Impact of membrane addition for effluent extraction on the performance and sludge characteristics of upflow anaerobic sludge blanket reactors treating municipal wastewater, *J. Membr. Sci.*, 479 (2015) 95–104.
- [30] L.G. Shen, Q. Lei, J.R. Chen, H.C. Hong, Y.M. He, H.J. Lin, Membrane fouling in a submerged membrane bioreactor: impacts of floc size, *Chem. Eng. J.*, 269 (2015) 328–334.
- [31] Z.Z. Wang, Y. Ji, L.N. Yan, D. Zhao, K. Zhang, W. Zhang, S.M. Li, Performance and fouling behaviors in a membrane-assisted biological nutrient removal process with focus on the effect of influent COD/N ratio, *Desal. Water Treat.*, 110 (2018) 76–88.
- [32] R. Chen, Y.L. Nie, Y.S. Hu, R. Miao, T. Utashiro, Q. Li, M.J. Xu, Y.Y. Li, Fouling behaviour of soluble microbial products and extracellular polymeric substances in a submerged anaerobic membrane bioreactor treating low-strength wastewater at room temperature, *J. Membr. Sci.*, 531 (2017) 1–9.

- [33] D.W. Gao, Y. Fu, N.Q. Ren, Tracing biofouling to the structure of the microbial community and its metabolic products: a study of the three-stage MBR process, *Water Res.*, 47 (2013) 6680–6690.
- [34] L. Duan, W. Jiang, Y.H. Song, S.Q. Xia, S.W. Hermanowicz, The characteristics of extracellular polymeric substances and soluble microbial products in moving bed biofilm reactor-membrane bioreactor, *Bioresour. Technol.*, 148 (2013) 436–442.
- [35] J.H. Teng, L.G. Shen, Y.C. Xu, Y.F. Chen, X.L. Wu, Y.M. He, J.R. Chen, H.J. Lin, Effects of molecular weight distribution of soluble microbial products (SMPs) on membrane fouling in a membrane bioreactor (MBR): novel mechanistic insights, *Chemosphere*, 248 (2020) 126013–126024.
- [36] H.F. Zhang, B.S. Sun, X.H. Zhao, Z.H. Gao, Effect of ferric chloride on fouling in membrane bioreactor, *Sep. Purif. Technol.*, 63 (2008) 341–347.
- [37] J.C. Baudez, P. Slatter, N. Eshtiaghi, The impact of temperature on the rheological behaviour of anaerobic digested sludge, *Chem. Eng. J.*, 215 (2013) 182–187.
- [38] J.L. Liang, S.W. Zhang, J.J. Huang, M.Y. Ye, X. Yang, S.S. Huang, S.Y. Sun, Mechanism of zero valent iron and anaerobic mesophilic digestion combined with hydrogen peroxide pretreatment to enhance sludge dewaterability: relationship between soluble EPS and rheological behavior, *Chemosphere*, 247 (2020) 125859–125871.
- [39] G. Sabia, M. Ferraris, A. Spagni, Effect of solid retention time on sludge filterability and biomass activity: longterm experiment on a pilot-scale membrane bioreactor treating municipal wastewater, *Chem. Eng. J.*, 221 (2013) 176–184.
- [40] Z.C. Wu, Z.W. Wang, Z. Zhou, G.P. Yu, G.W. Gu, Sludge rheological and physiological characteristics in a pilot-scale submerged membrane bioreactor, *Desalination*, 212 (2007) 152–164.
- [41] J.P. Croué, M.F. Benedetti, D. Violleau, J.A. Leenheer, Characterization and copper binding of humic and nonhumic organic matter isolated from South Platte River: evidence for the presence of nitrogenous binding site, *Environ. Sci. Technol.*, 37 (2003) 328–336.
- [42] M. Kumar, S.S. Adham, W.R. Pearce, Investigation of seawater reverse osmosis fouling and its relationship to pretreatment type, *Environ. Sci. Technol.*, 40 (2006) 2037–2044.